Int. J. Electrochem. Sci., 7 **(2012)** 11617 - 11633

International Journal of
ELECTROCHEMICAL
SCIENCE
www.electrochemsci.org

Corrosion Behavior of Ceftibuten in Hydrochloric Acid Solution

Ashish Kumar Singh[1,*], *Chitrasen Gupta*[2], *Eno E. Ebenso*[1]

[1] Department of Chemistry, School of Mathematical & Physical Sciences, North West University (Mafikeng Campus), Private Bag X2046, Mmabatho 2735, South Africa
[2] Department of Chemistry, Kutir P. G. College, Chakke, Jaunpur, India
[*]E-mail: singhapc@gmail.com

Received: 27 July 2012 / *Accepted:* 30 September 2012 / *Published:* 1 November 2012

The inhibition effect of ceftibuten (CBT) on the corrosion behavior of mild steel (MS) in 1 M HCl solution was studied using potentiodynamic polarization, electrochemical impedance spectroscopy (EIS) and weight loss techniques. The surface morphology of the MS after its exposure to 1 M HCl solution with and without 100 ppm CBT was examined by scanning electron microscopy (SEM) and atomic force microscopy (AFM). The value of activation energy (E_a), Arrhenius factor, enthalpy and entropy for the MS corrosion and the thermodynamic parameters such as adsorption equilibrium constant (K_{ads}), free energy of adsorption (ΔG^0_{ads}), adsorption heat (ΔH^0_{ads}) and adsorption entropy (ΔS^0_{ads}) values were calculated and discussed. The adsorption behavior of CBT is experimentally investigated by contact angle measurement on mild steel surface. The hydrophobic character of MS increased with increasing concentration of CBT. The results showed that CBT performed excellent inhibiting effect for the corrosion of the MS.

Keywords: Corrosion inhibitors; Adsorption; AFM; EIS

1. INTRODUCTION

Corrosion is a fundamental process playing an important role in economics and safety, particularly for metals and alloys. Steel has found wide application in a broad spectrum of industries and machinery; however its tendency to corrosion. The corrosion of steel is a fundamental academic and industrial concern that has received a considerable amount of attention. Among several methods used in combating corrosion problems, the use of chemical inhibitors remains the most cost effective and practical method. Therefore, the development of corrosion inhibitors based on organic compounds containing nitrogen, sulphur and oxygen atoms are of growing interest in the field of corrosion and

industrial chemistry as corrosion poses serious problem to the service lifetime of alloys used in industry [1].

Many corrosion inhibitors used in aqueous heating and cooling systems are generally toxic and generate health hazards. This toxic property limits the field of their applications. However there is a great demand for nontoxic corrosion inhibitors. The development of new corrosion inhibitors of non-toxic type, which do not contain heavy metals and organic phosphates, remains very important.

Ceftibuten is the commercial name of (6R, 7R)-7-([(Z)-2-(2-amino-1,3-thiazol-4-yl)-5-hydroxy-5-oxopent-2-enoyl]amino) -8-oxo-5-thia-1-azabicyclo[4.2.0]oct-2-ene-2-carboxylic acid. It is a third-generation cephalosporin antibiotic.

This paper reported our attempt to use electrochemical impedance spectroscopy (EIS), potentiodynamic polarization, weight loss, atomic force microscopy (AFM), scanning electron microscopy (SEM) and contact angle measurement to investigate the nature of adsorption of ceftibuten (CBT) on the mild steel surface. The structure of CBT is shown in Fig. 1.

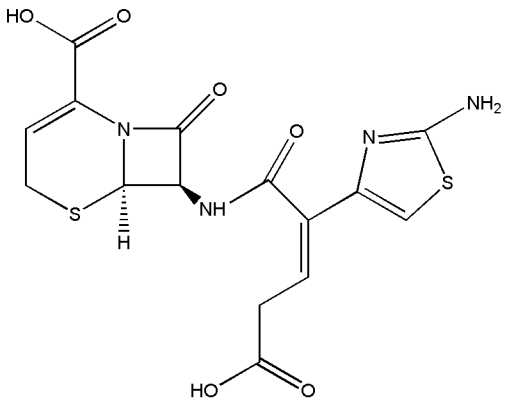

Figure 1 Structure of ceftibuten (CBT) molecule

2. EXPERIMENTAL

2.1. Inhibitor

Stock solution of CBT was made in 10:1 ratio water: ethanol mixture to ensure solubility. This stock solution was used for all experimental purposes.

2.2. Mild steel sample

The chemical composition of the working electrode, a mild steel electrode was determined as (wt. %) C = 0.17, Mn = 0.46, Si = 0.26, S = 0.017, P = 0.019 and balance Fe. It was mechanically ground with 320, 400, 600, 800, 1000 and 1200 emery paper, washed in acetone and bidistilled water then dried and put into the cell.

2.3. Electrochemical measurements

A three-electrode cell consisting of carbon steel working electrode

(WE), a platinum counter electrode (CE) and saturated calomel electrode (SCE) as a reference electrode, was used for electrochemical measurements. All experiments were performed in atmospheric condition without stirring. Prior to the electrochemical measurement, a stabilization period of 30 min was allowed, which was proved to be sufficient to attain a stable value of E_{corr}.

The EIS measurements were carried out in a frequency range from 100 kHz to 0.00001 kHz under potentiodynamic conditions, with amplitude of 10 mV peak-to peak, using AC signal at E_{corr}.

The potentiodynamic polarization curves were recorded in the potential range of -250 to +250 mV (SCE) with scan rate 1 mV s^{-1}. All potentials were measured against SCE.

2.4. Weight loss measurements

Weight loss experiments were done according to the method described previously [2]. Weight loss measurements were performed at 308 K for 3 h by immersing the mild steel coupons into acid solution (100 mL) without and with various amounts of inhibitors. After the elapsed time, the specimen were taken out, washed, dried and weighed accurately.

The inhibition efficiency ($\mu_{WL}\%$) and surface coverage (θ) was determined by using following equations:

$$\mu_{WL}\% = \frac{w_0 - w_i}{w_0} \times 100 \quad (1)$$

$$\theta = \frac{w_0 - w_i}{w_0} \quad (2)$$

Where, w_0 and w_i are the weight loss value in the absence and presence of inhibitor.

2.5. Scanning electron microscopy (SEM)

The carbon steel specimens (size 1.0 cm × 1 cm × 0.025 cm) were abraded with emery paper (grade 320–400–600–800–1000–1200) then were washed with distilled water and acetone. After immersion in 1 M HCl without and with addition of 100 ppm of CBT at 308 K for 3 h, steel specimens were cleaned with distilled water; dried using a cold air blaster, and then the surface was investigated by a Jeol JSM-5400 (SEM).

2.6. Atomic force microscopy (AFM)

The surface morphology of mild steel specimen was investigated by using atomic force microscope (AFM). Atomic force microscopy was performed using a NT-MDT multimode AFM,

Russia, controlled by Solver scanning probe microscope controller. Semi-contact mode was used with the tip mounted on 100 μm long, single beam cantilever with resonant frequency in the range of 2.4×10^5-2.5×10^5 Hz, and the corresponding spring constant of 11.5 N m^{-1} with NOVA programme used for image rendering [3]. The mild steel strips of $1.0 \times 1.0 \times 0.025$ cm sizes were prepared as described in section 2.5. After immersion in 1 M HCl with and without addition of 100 ppm of CBT at 308 K for 3 h, the specimen were cleaned with distilled water, dried and then used for AFM.

2.7. Contact angle measurements (static sessile drop method)

For the measurements of the contact angle, the mild steel samples above described were used. Prior to any contact angle measurements, the mild steel coupons were carefully cleaned in order to remove surface contamination like grease, dust or organic traces that could influence contact angle measurements through surface pinning of the liquid drop and or contamination of the liquid when the latter is put into contact with the sample surface. Aqueous acid solutions with different concentrations of the CBT were prepared and the samples were then immersed into these solutions for 3 h. Upon removal from the solutions, the samples were dried by means of gently nitrogen flow. Contact angle measurements were performed using the static sessile drop method with a Rame-Hart goniometer (Netcong, USA).

3. RESULTS AND DISCUSSION

3.1. Electrochemical impedance spectroscopy (EIS)

Impedance method provides information about the kinetics of the electrode processes and simultaneously about the surface properties of the investigated systems. The shape of impedance gives mechanistic information. The method is widely used for investigation of the corrosion inhibition processes [4 Singh AK, Quraishi MA, Ebenso EE (2011) Inhibitive Effect of Cefuroxime on the Corrosion of Mild Steel in Hydrochloric Acid Solution. Int. J. Electrochem. Sci. 6:5676-5688, Singh AK, (2012) Inhibition of Mild Steel Corrosion in Hydrochloric Acid Solution by 3-(4-((Z)-Indolin-3-ylideneamino) phenylimino) indolin-2-one. Ind Engg Chem Res 51:3215-3223]. Nyquist and Bode plots of mild steel in 1 M HCl solution in absence and presence of different concentrations of CBT are presented in Fig. 2a-b. It follows from Fig. 2a that a high frequency (HF) depressed charge-transfer semicircle was observed (one time constant in Bode plot) followed by a well defined inductive loop in the low frequency (LF) regions. The HF semicircle is attributed to the time constant of charge transfer and double-layer capacitance [7, 8]. The LF inductive loop may be attributed to the relaxation process obtained by adsorption species as Cl^-_{ads} and H^+_{ads} on the electrode surface [9].

Phase angle at high frequencies provided a general idea of anticorrosion performance. The more negative the phase angle the more capacitive the electrochemical behavior [10]. Charge transfer resistance increment could raise current tendency to pass through the capacitor in the circuit. Also, depression of phase angle at relaxation frequency with decreasing the CBT concentration (Fig. 2c)

indicated the decrease of capacitive response with the decrease of inhibitor concentration. Such a phenomenon could be attributed to higher corrosion activity at low concentrations of inhibitor.

In the Bode magnitude diagram (Fig. 2b) one slope can be identified; moreover the first derivative curve obtained from this diagram shows only one maxima confirming the presence of one time constant (Fig. 2d)

To get more accurate fit of these experimental data, the measured impedance data were analyzed by fitting in to equivalent circuit given in Fig. 2e Excellent fit with this model was obtained for all experimental data. The equivalent circuit consists of the double-layer capacitance (Q) in parallel to the charge transfer resistance (R_{ct}), which is in series to the parallel of inductive elements (L) and R_L. The presence of L in the impedance spectra in the presence of the inhibitor indicates that mild steel is still dissolved by the direct charge transfer at the CBT-adsorbed mild steel surface [11].

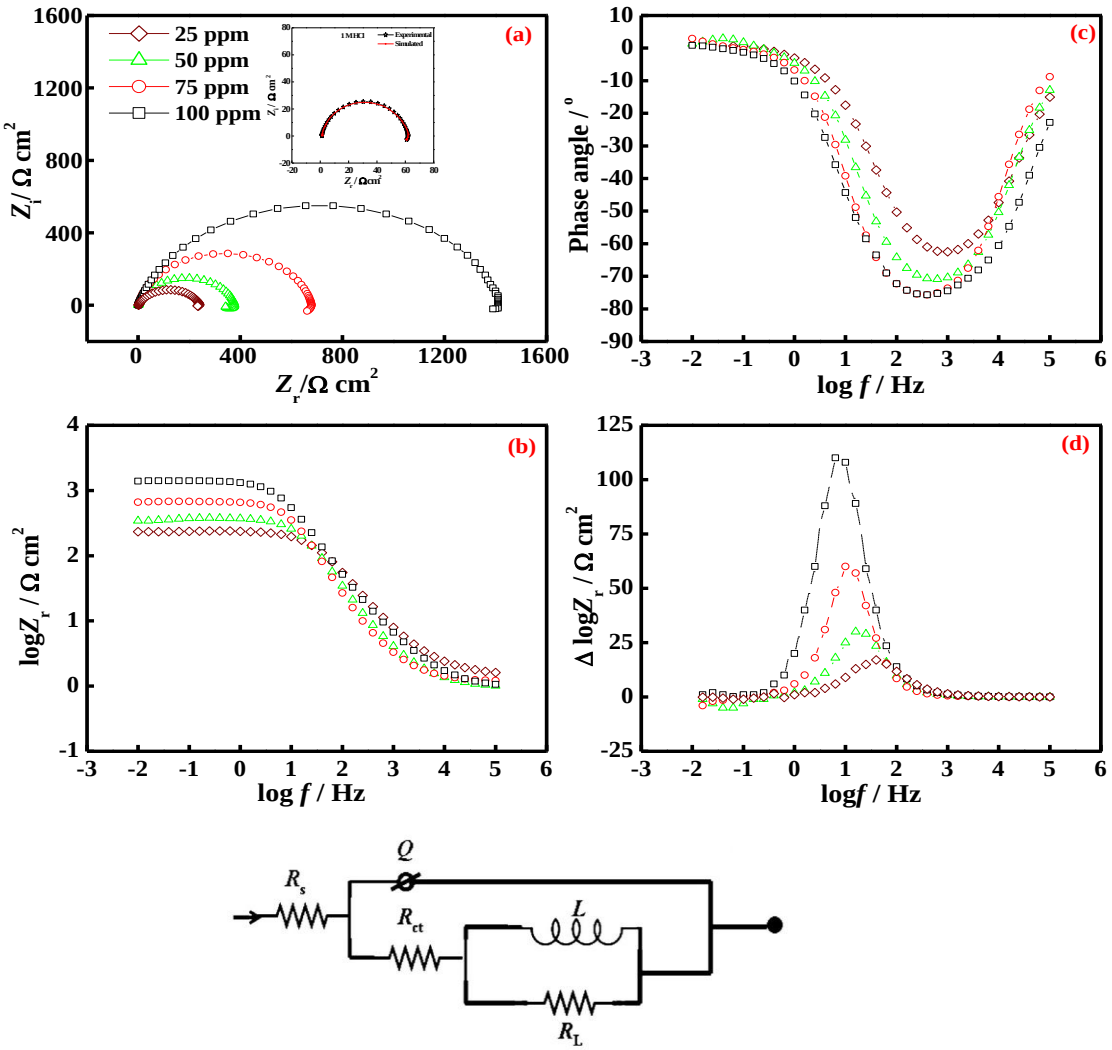

(e)

Figure 2. (a) Nyquist plots, (b) Bode-magnitude plots, (c) Phase angle plots, (d) differential magnitude diagram, of the corrosion product films obtained in absence and presence of different concentration of CBT and (e) The electrochemical equivalent circuit used to fit the impedance measurements

Table 1. Electrochemical impedance parameters of mild steel in 1 M HCl in absence and presence of different concentrations of CBT

Conc. of inhibitor / ppm	Temperature / K	Q / Ω^{-1} s^n cm^{-2}	n	R_{ct} / Ω cm	R_L / Ω cm^2	L / H	E_{EIS}%
-	308	56.9	0.786	51.5	7.5	8.7	-
25	308	50.8	0.825	231.5	9.5	13.9	77.7
50	308	44.5	0.849	339.1	41.2	49.6	84.8
75	308	35.2	0.892	601.7	77.3	61.6	91.4
100	308	29.0	0.921	1368.0	52.4	81.8	96.2

One constant phase element (CPE) is substituted for the capacitive element to give a more accurate fit, as the obtained capacitive loop is a depressed semi-circle. The depression in Nyquist semicircles is a feature for solid electrodes and often referred to as frequency dispersion and attributed to the roughness and other inhomogenities of the solid electrode [12]. The CPE is a special element whose admittance value is a function of the angular frequency (ω), and whose phase is independent of the frequency. The admittance and impedance of CPE is given by;

$$Y_{CPE} = Y_0(i\omega)^n \quad (3)$$

where, Y_0 is the magnitude of CPE, i is an imaginary number ($i^2 = -1$) α is the phase angle of CPE and $n = \alpha/(\pi/2)$ in which α is the phase angle of CPE. The point of intersection between the inductive loop and the real axis represents ($R_s + R_{ct}$). The electrochemical parameters, Including R_s, R_{ct}, R_L, L, Y_0 and n, obtained from fitting the recorded EIS using the electrochemical circuit of Fig. 2e are listed in Table 1. C_{dl} values derived from CPE parameters according to equation (4) listed in Table 1.

$$C_{dl} = Y_0(\omega_{max})^{n-1} \quad (4)$$

Where, ω_{max} is angular frequency ($\omega_{max} = 2\pi f_{max}$) at which the imaginary part of impedance ($-Z_i$) is maximal and f_{max} is AC frequency at maximum.

3.2. Potentiodynamic polarization curves

The current–potential relationships (cathodic and anodic) for mild steel in 1 M HCl in the absence and presence different concentrations of CBT at all studied temperature are shown in Fig. 3. Values of associated electrochemical parameters such as corrosion potential (E_{corr}), corrosion current density (Icorr), anodic and cathodic Tafel slopes (b_a, b_c) and the calculated μ_p% are presented in Table 2. In this case, the inhibition efficiency is defined as follows:

$$\mu_{\mathrm{P}}\% = \frac{I_{\mathrm{corr}}^{0} - I_{\mathrm{corr}}^{\mathrm{i}}}{I_{\mathrm{corr}}^{0}} \times 100 \qquad (5)$$

Where, I_{corr}^{0} and $I_{\mathrm{corr}}^{\mathrm{i}}$ are the corrosion current density in absence and presence of inhibitor respectively.

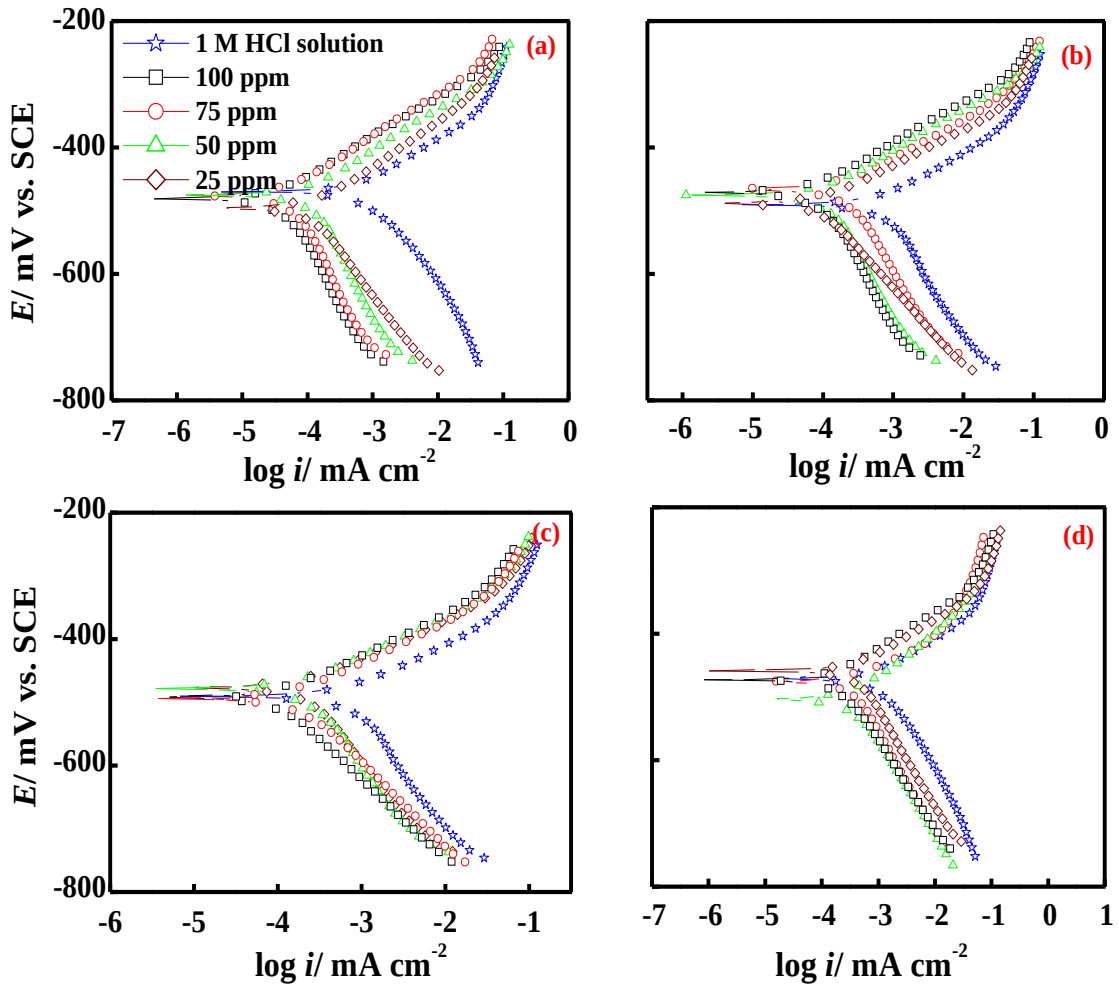

Figure 3 Typical polarization curves for corrosion of mild steel in 1 M HCl in the absence and presence of different concentrations of CBT at different temperature

Close examination of Table 2 shows that an increase in temperature increases I_{corr}, while the addition of CBT decreases the I_{corr} values across the temperature range. The results also indicate that the inhibition efficiencies increased with the concentration of inhibitor but decreased proportionally with temperature. Such behavior can be interpreted on the basis that the inhibitor acts by adsorbing onto the metal surface, and an increase in temperature results in desorption of some adsorbed inhibitor molecules, leading to a decrease in the inhibition efficiency [13].

The potentiodynamic curves show that there is a clear reduction of both the anodic and cathodic currents in the presence of CBT compared with those for the blank solution. It is clear that the

cathodic reaction (hydrogen evolution) and the anodic reaction (dissolution metal) were inhibited. The values of cathodic Tafel slope (b_c) for CBT influence the kinetics of the hydrogen evolution reaction [14]. This indicates an increase in the energy barrier for proton discharge, leading to less gas evolution [15]. The approximately constant values of anodic Tafel slope (b_a) for CBT indicate that CBT was first adsorbed onto the metal surface and impeded by merely blocking the reaction sites of the metal surface without affecting the anodic reaction mechanism [16]. There was no definite trend is observed in the E_{corr} values in the presence of CBT. In the present study, shift in E_{corr} values is in the range of 3-35 mV suggested that CBT acted as mixed type of inhibitor [17, 18]

Table 2. Potentiodynamic polarization parameters for the corrosion of mild steel in 1 M HCl in absence and presence of different concentrations of CBT at different temperature

Conc. of inhibitor / ppm	Temperature / K	$-E_{corr}$ / /mV *vs.* SCE	I_{corr} / μA cm^{-2}	b_a / mV/dec	b_c / mV/dec	E_p %
-	308	466	668	67	137	-
25	308	496	168	79	222	75
50	308	475	146	81	247	78
75	308	475	71	85	246	89
100	308	481	45	76	198	93
-	318	490	752	74	154	-
25	318	466	249	74	212	67
50	318	475	155	82	255	79
75	318	488	110	66	160	85
100	318	471	90	75	181	88
-	328	490	774	76	161	-
25	328	477	301	75	259	61
50	328	478	237	74	177	69
75	328	494	180	74	166	77
100	328	491	132	71	177	83
-	338	471	848	60	114	-
25	338	503	390	73	153	54
50	338	476	331	58	152	61
75	338	459	250	68	150	70
100	338	473	211	69	139	75

3.3. Effect of temperature on the corrosion current

To investigate the mechanism of inhibition and to calculate the activation energies of the corrosion process, polarization measurements were taken at various temperatures in the absence and the presence of different concentrations of CBT. Corresponding data are given in Table 3. In the studied temperature range (303-338 K) the corrosion current density increases with increasing temperature both in uninhibited and inhibited solutions and the values of the inhibition efficiency of CBT are nearly constant. The corrosion current density of steel increases more rapidly with temperature in the absence of the inhibitor, these results confirm that CBT acts as an efficient inhibitor in the range of temperature studied. The CBT inhibitor efficiency was temperature independent.

The activation parameters for the corrosion process were calculated from Arrhenius type plot according to the following equation:

$$\log I_{corr} = -\frac{E_a}{2.303RT} + \log \lambda \quad (6)$$

and from transition state plot according to the following equation:

$$\log \frac{I_{corr}}{T} = \frac{RT}{Nh} \exp\left(\frac{\Delta S^*}{R}\right) \exp\left(-\frac{\Delta H^*}{RT}\right) \quad (7)$$

where, E_a is the activation energy, R is gas constant, h is Planck's constant, T is absolute temperature, λ is Arrhenius pre-exponential factor, ΔH^* is enthalpy of activation and ΔS^* is entropy of activation.

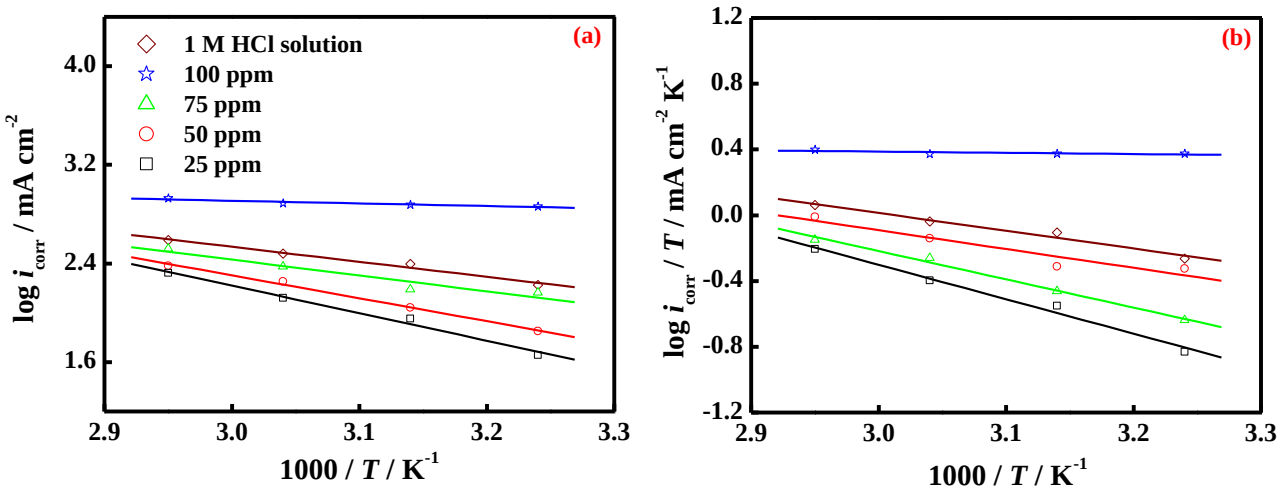

Figure 4. Arrhenius plots in absence and presence of different concentration of CBT for (a) log C_R versus 1/T and (b) log (C_R/T) versus 1/T

Table 3. Thermodynamic activation parameters for mild steel in 1 M HCl in absence and presence of different concentrations of CBT

Conc. of inhibitor (ppm)	E_a (kJ mol^{-1})	λ (mmy^{-1})	ΔH^* (kJ mol^{-1})	ΔS^* (J mol^{-1} K^{-1})
-	20.06	3.51×10^3	1.41	-80.75
25	23.30	1.53×10^6	20.65	-135.39
50	24.50	1.92×10^6	21.92	-133.52
75	35.60	7.65×10^7	32.95	-102.85
100	42.80	8.44×10^8	40.14	-82.94

The apparent activation energy and pre-exponential factors for a wide range of concentration of the inhibitor can be calculated by linear regression between $\log I_{corr}$ and $1/T$, the results were shown

in Table 3. All the linear regression coefficients are close to 1, indicating that corrosion of mild steel in 1 M HCl can be explained using the kinetic model. Fig. 4a depicted an Arrhenius plots for mild steel immersed in 1 M HCl in presence of different concentration of CBT. The plots obtained are straight lines and the slope of each straight line gives its apparent activation energy. Table 3 presented E_a and λ values for a wide range of concentration of CBT. Inspection of Table 3 showed that apparent activation energy increased on addition of CBT in comparison to the blank solution. The increase in E_a could be interpreted as the physical adsorption. Szauer and Brandt [19] explained that the increase in activation energy can be attributed to an appreciable decrease in the adsorption of the inhibitor on the mild steel surface with increase in temperature and a corresponding increase in corrosion current density occurs due to the fact that greater area of metal is exposed to the acid environment.

According to equation (6), corrosion current density (I_{corr}) is being affected by both E_a and λ. In general, the influence of E_a on the mild steel corrosion is higher than that of λ. However, if the variation in λ was drastically higher than that of E_a, the value of λ might be the dominant factor to determine the mild steel corrosion. In present case, E_a and λ increased with concentration (the higher E_a and lower λ led to lower corrosion current density). As it can be seen from Fig. 3, the corrosion current density of steel decreased with increasing concentration; hence, it is clear that increment of E_a is the decisive factor affecting the corrosion current density of mild steel in 1 M HCl.

The relationship between $\log(I_{corr}/T)$ and $1/T$ were shown in Fig. 4b. Straight lines are obtained with a slope $(-\Delta H^*/2.303R)$ and an intercept of $\left[\log(R/Nh)+(\Delta S^*/2.303R)\right]$, from which the value of ΔH^* and ΔS^* were calculated and presented in Table 3. The positive sign of enthalpy reflect the endothermic nature of steel dissolution process meaning that dissolution of steel is difficult. On comparing the values of entropy of activation (ΔS^*) listed in Table 3, it is clear that entropy of activation increased in presence of the studied inhibitor compared to free acid solution. Such variation is associated with the phenomenon of ordering and disordering of inhibitor molecules on the mild steel surface. The increased entropy of activation in the presence of inhibitor indicated that disorderness is increased on going from reactant to activated complex.

3.4. Adsorption isotherm

The adsorption on the corroding surfaces never reaches the real equilibrium and tends to reach an adsorption steady state. When corrosion rate is sufficiently decreased in the presence of inhibitor, the adsorption steady state has a tendency to attain quasi-equilibrium state. Now, it is reasonable to consider quasi-equilibrium adsorption in thermodynamic way using the appropriate adsorption isotherm. The degree of surface coverage (θ) for inhibitor was obtained from potentiodynamic polarization data. Different adsorption isotherms such as Langmuir, Temkin and Frumkin (Fig. 5a-c) were tested in order to find the best fit adsorption isotherm for adsorption of CBT on the surface of mild steel from 1 M HCl solution. Since, the linear regression coefficient of Langmuir adsorption isotherm is found more close to unity hence, was found best fit (Fig. 5a). With regard to the Langmuir

adsorption isotherm the surface coverage (θ) of the inhibitor on the mild steel surface is related to the concentration (C_{inh}) of the inhibitor in the bulk of the solution according to the following equation:

$$\theta = \frac{K_{ads} C_{inh}}{1 + K_{ads} C_{inh}} \quad (8)$$

where, K_{ads} is the equilibrium constant for the adsorption/desorption process. This equation can be rearranged to

$$\frac{C_{inh}}{\theta} = \frac{1}{K_{ads}} + C_{inh} \quad (9)$$

It is known fact that K_{ads} represents the strength between adsorbate and adsorbent. Large values of K_{ads} imply more efficient adsorption and hence better inhibition efficiency [20].

From the intercepts of the straight lines on the C_{inh}/θ-axis (Fig. 5a), K_{ads} can be calculated which is related to free energy of adsorption, ΔG^{o}_{ads} as given by equation (10).

$$\Delta G^{o}_{ads} = -RT \ln(55.5 K_{ads}) \quad (10)$$

The negative values of ΔG^{o}_{ads} ensure the spontaneity of the adsorption process and stability of the adsorbed film on the mild steel surface [21, 22]. It is usually accepted that the value of ΔG^{o}_{ads} around -20 kJ mol^{-1} or lower indicates the electrostatic interaction between charged metal surface and charged organic molecules in the bulk of the solution while those around -40 kJ mol^{-1} or higher involve charge sharing or charge transfer between the metal surface and organic molecules [23-26].

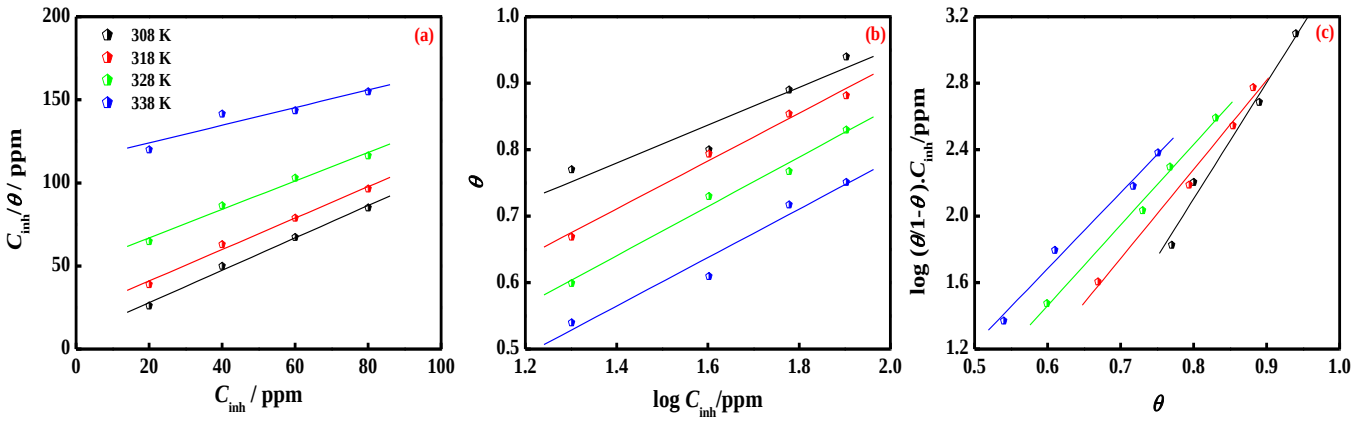

Figure 5. (a) Langmuir adsorption isotherm, (b) Temkin and (c) Frumkin adsorption isotherm

Table 4. Thermodynamic parameters for the adsorption of ceftibuten in 1 M HCl on the mild steel at different temperatures

Conc. of inhibitor (ppm)	Temperature (K)	K_{ads} ($104 \times M^{-1}$)	$-\Delta G^{o}_{ads}$ (kJ mol^{-1})	$-\Delta H^{o}_{ads}$ (kJ mol^{-1})	ΔS^{o}_{ads} (J K^{-1} mol^{-1})
100	308	6.65	38.7	46.02	-57.36
	318	3.16	38.0		
	328	2.07	38.4		
	338	1.28	37.8		

Assuming thermodynamic model, corrosion inhibition of mild steel in the presence of CBT can be better explained, therefore, heat of adsorption and entropy of adsorption were calculated.

According to Van't Hoff equation [27]:

$$\ln K_{ads} = \frac{-\Delta H^{o}_{ads}}{RT} + \text{constant} \qquad (11)$$

To calculate heat of adsorption $\ln K_{ads}$ was plotted against $1/T$, as shown in Fig. 6. The straight lines were obtained with slope equal to $(-\Delta H^{o}_{ads}/R)$ and intercept equal to $(\Delta S^{o}_{ads}/R + \ln 1/55.5)$. The calculated values of heat of adsorption and entropy of adsorption are listed in Table 4. Under the experimental conditions, the adsorption heat could be approximately regarded as the standard adsorption heat (ΔH^{o}_{ads}).

3.5. Weight loss measurements

Fig. 7a represented variation of inhibition efficiency as a function of concentration of CBT, immersion time and acid concentration. Fig. 8a showed that inhibition efficiency of CBT increased as the conc. increases, led to conclusion that as the conc. of CBT increases, it is more available to adsorb on the mild steel surface and resulting in to inhibition of corrosion.

Fig. 7b represented inhibition efficiency *vs.* immersion time. As from the Fig. 8b, inhibition efficiency increased first from 3-12 h and thereafter almost constant. It can be concluded that persistent film formation is a function of time.

Fig. 7c showed plot of inhibition efficiency *vs.* acid concentration. It can be seen that inhibition efficiency is almost constant (decreased 1-1.5%) by increasing acid concentration from 0.5 M to 2.0 M. Thus, CBT behaved as an efficient inhibitor under the studied acid concentration range.

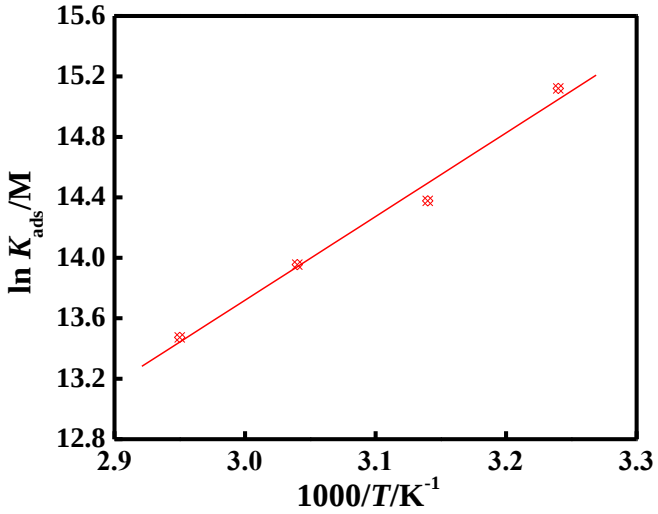

Figure 6. Adsorption isotherm plot for ln K_{ads} *vs.* 1/T

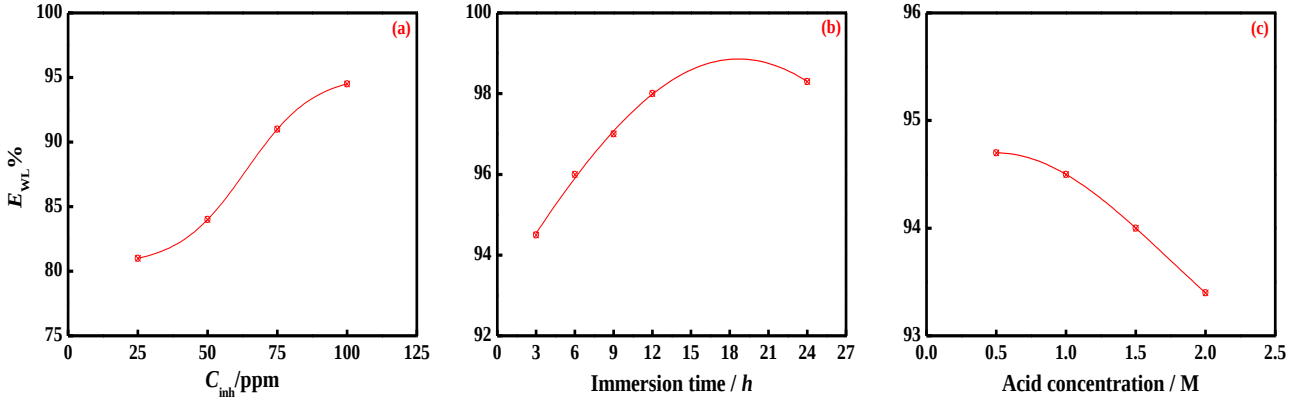

Figure 7. Variation of inhibition efficiency obtained from weight loss measurements with (a) concentration of CBT, (b) immersion time and (c) acid concentration

3.6. Scanning electron microscopy (SEM)

The SEM images of mild steel surfaces are given in Fig. 8 a-c. The inspection of Fig. 8a, which is the micrograph of the mild steel surfaces exposed to 1 M HCl revealed that the specimen surface was strongly damaged in the absence of inhibitor. Fig. 8b showed the SEM image of the mild steel surface exposed to the 1 M HCl with the addition of 100 ppm CBT. There are no pits and cracks observed in the micrograph except polishing lines. The Fig. 8c showed polished mild steel surface.

3.7. Atomic force microscopy (AFM)

AFM is a powerful technique to investigate the surface morphology at nano to micro-scale and has become a new choice to study the influence of inhibitor on the generation and the progress of the

corrosion at the metal/solution interface. Analysis of the images allowed quantification of surface roughness over area scales 12 × 12 μm^2. Atomic force microscope was used mainly for measuring three-dimensional topography. The three-dimensional AFM images are shown in Fig. 8 d-f. The average roughness of bare mild steel surface was calculated as 65 nm (Fig. 8d) and the average roughness of mild steel in 1 M HCl without inhibitor (Fig. 8e) was calculated as 505 nm.

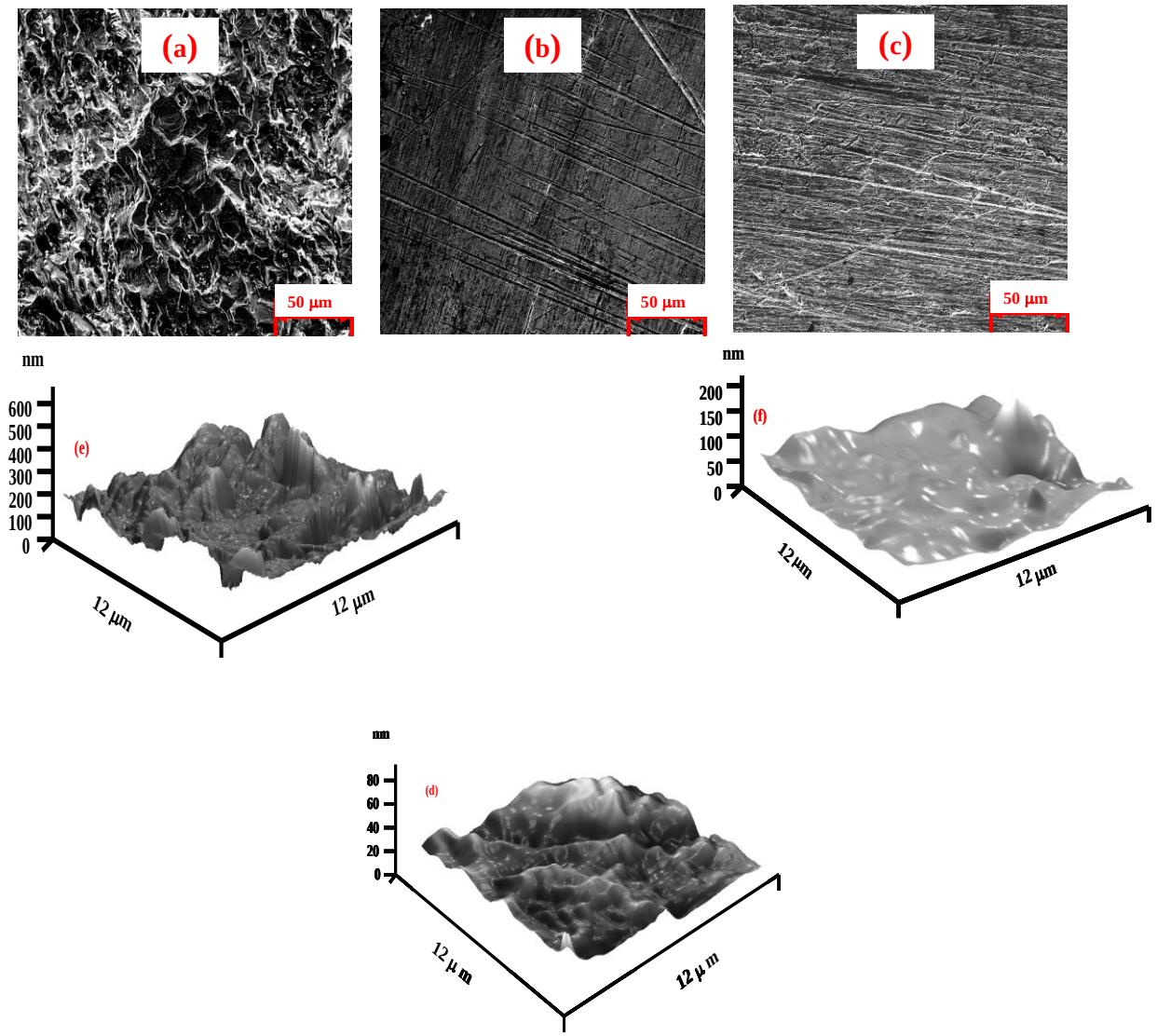

Figure 8 (a) Scanning electron micrograph of mild steel surface exposed to free acid solution and (b) scanning electron micrograph of inhibited mild steel (1 M HCl + 100 ppm CBT), (c) scanning electron micrographs of polished mild steel surface, (d) atomic force micrograph of polished mild steel surface, (e) atomic force micrograph of mild steel surface exposed to free acid solution and (f) atomic force micrograph of inhibited mild steel surface (1 M HCl + 100 ppm CBT)

The mild steel in the free acid solution is getting cracked due to due to acid attack on the surface (Fig. 8e). However, in presence of 200 ppm of inhibitor the average roughness was reduced to 137 nm (Fig. 8f).

3.8Contact angle of acid solution on mild steel surface

Fig. 9 displays the contact angle, θ, as a function of CBT concentration for acid solutions on mild steel. For acid solution without inhibitor, contact angle, θ, is lowest (14.7) thereby metal showing most hydrophilic nature. As the concentration of inhibitor increases, contact angle regularly increases. By increasing contact angle, metal showed hydrophobic character to the acid solution containing inhibitor. The contact angle increased regularly with increasing concentration of inhibitor.

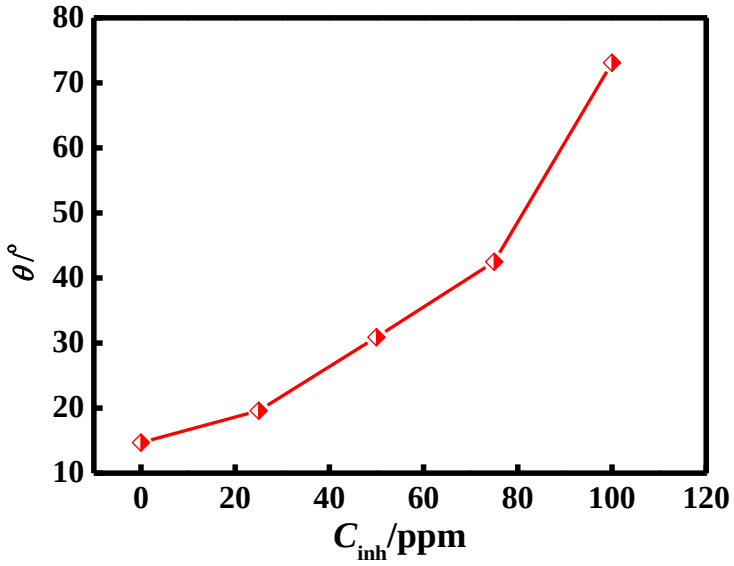

Figure 9 Contact angle, θ, of acid solutions containing different concentrations of CBT on mild steel surface

4. MECHANISM OF INHIBITION

It has been assumed that organic inhibitor molecule establish its inhibition action via the adsorption of the inhibitor onto the metal surface. The adsorption process is affected by the chemical structures of the inhibitors, the nature and charged surface of the metal and the distribution of charge over the whole inhibitor molecule. In general, owing to the complex nature of adsorption and inhibition of a given inhibitor, it is impossible for single adsorption mode between inhibitor and metal surface.

The adsorption and inhibition effect of CBT in HCl solution can be explained as follows: CBT might be protonated in the acid solution as following:

$$CBT+xH^{+} \leftrightarrow [CBT_x]^{x+} \quad (12)$$

Thus, in aqueous acidic solutions, the CBT exists either as neutral molecules or in the form of cations (protonated CBT). Generally, two modes of adsorption could be considered. The neutral CBT

may be adsorbed on the metal surface via the chemisorption mechanism, involving the displacement of water molecules from the metal surface and the sharing electrons between the N atoms and iron. The CBT molecules can be also adsorbed on the metal surface on the basis of donor–acceptor interactions between π-electrons of nitrile group and carbonyl group and vacant d-orbital of iron. Instead of this dπ-dπ bonds are also formed by the overlap of 3d-electrons of Fe-atom to vacant 3d-orbital of S-atom. In another hand, it is well known that the steel surface charges positive charge in acid solution [28], so it is difficult for the protonated CBT to approach the positively charged steel surface (H_3O^+/metal interface) due to the electrostatic repulsion. Since chloride ions have a smaller degree of hydration, being specifically adsorbed, they create an excess negative charge towards the solution and favour more adsorption of the cations [22], the protonated CBT may adsorb through electrostatic interactions between the positively charged molecules and the negatively charged metal surface.

5. CONCLUSIONS

1. The obtained results showed that CBT performed perfect inhibition efficiency for the corrosion of the MS in 1 M HCl solution and the inhibition efficiency was more pronounced with inhibitor concentration and exposure time.

2. The adsorption of CBT molecules on the metal surface from 1 M HCl solution obeyed Langmuir adsorption isotherm. The negative sign of ΔG^{o}_{ads} and ΔH^{o}_{ads} indicate that the adsorption process is spontaneous and exothermic.

3. The contact angle increased with increasing concentration of inhibitor confirming the hydrophobic behavior.

4. Potentiodynamic polarization revealed that CBT acted as mixed type of inhibitor predominantly cathodic.

References

1. E.E. Oguzie, Y. Lia, F.H. Wang, *Electrochim Acta* 53(2007)909-914
2. A.K. Singh, M.A. Quraishi, *J. Appl. Electrochem.* 41 (2011) 7-18
3. A.K. Singh, M.A. Quraishi, *Corros. Sci.* 53 (2011) 1288-1297
4. V.P. Singh, P. Singh, A.K. Singh, *Inorg Chim Acta* 379 (2011) 56-63
5. A.K. Singh, M.A. Quraishi, E.E Ebenso, *Int. J. Electrochem. Sci.* 6 (2011) 5676-5688,
6. A.K. Singh, *Ind. Eng. Chem. Res.* 51 (2012) 3215-3223
7. C. Deslouis, B. Tribollet, G. Mengoli, M.M. Musiani, *J. Appl. Electrochem.* 18 (1988)374-383
8. S.S. Abdel Rehim, H.H. Hassan, M.A. Amin, *Appl. Surf. Sci.*, 187 (2002) 279-290.
9. A.k. Singh, M.A. Quraishi, *Corros Sci* 5 2(2010) 1373-1385
10. A.K. Singh, M.A Quraishi, *Mater. Chem. Phys.* 123 (2010) 666-677
11. A.K. Singh , M.A. Quraishi, *J. Appl. Chem.* 40 (2010) 1293-1306.
12. M. Mahadavian, M.M. Attar, *Corros. Sci.* 48 (20006) 4152-4157.
13. R. Solmaz, G. Kardas, M. Culha, B. Yazıcı, M. Erbil, *Electrochim. Acta*, 53 (2008) 5941-5952
14. G. Quartarone, L. Bonaldo, C. Tortato, *Appl. Surf. Sci.*, 252 (2006) 8251-8257
15. S.T. Selvi, V. Raman, N. Rajendran, *J. Appl. Electrochem*. 33 (2007) 1175-1182

16. A.K. Singh, M.A. Quraishi, *Int.J. Electrochem. Sci.* 7 (2012) 3222-3241
17. A.K. Singh, E.E. Ebenso, M.A. Quraishi, *Int. J. Electrochem. Sci*. 7 (2012) 2320-2333
18. A.K. Singh, M.A. Quraishi, *Corros. Sci*. 52 (2010) 1529-1533
19. A.K. Singh, S. Khan, A. Singh, S.M. Quraishi, M.A. Quraishi, *Res. Chem. Intermed.* DOI 10.1007/s11164-012-0677-8
20. A.K. Singh, S.K. Shukla, M. Singh, M.A. Quraishi, *Mater. Chem. Phys.* 129 (20110 68-76
21. O.L. Jr Riggs, Corrosion Inhibitors, 2nd ed., C.C. Nathan, Houston, TX p109, 1973
22. T. Szauer, A. Brandt, *Electrochim. Acta*, 26 (1981) 1257–1260
23. [A.K. Singh, M.A Quraishi, *Corros. Sci.*, 52 (2010) 152-160
24. H. Keles, M. Keles, I. Dehri, O. Serindag, *Colloids Surf A: Physicochem Eng Aspects* 320 (2008) 138-145
25. A.K. Singh, M.A. Quraishi, *Corros. Sci*., 51 (2009) 2752-2760
26. F. Bentiss, C. Jama, B. Mernari, H. El Attari, L. El Kadi, M. Lebrini, M. Traisnel, M. Lagrenee, *Corros. Sci.*, 51 (2009)1628-1635
27. X. Li, L. Tang, *Mater. Chem. Phys.* 90 (2005) 286-297.
28. L. B. Tang, X. Li, L. Li, G. Mu, G. Liu, *Surf. Coat. Technol.* 201 (2006) 384-388